Planetary and Space Science 85 (2013) 243–249

Contents lists available at ScienceDirect

Planetary and Space Science

journal homepage: www.elsevier.com/locate/pss

Night and day airglow of oxygen at 1.27 μm on Mars

Vladimir A. Krasnopolsky [a,b,*,1]

[a] Department of Physics, Catholic University of America, Washington, DC 20064, USA
[b] Moscow Institute of Physics and Technology, Dolgoprudnyy 141700, Russia

ARTICLE INFO

Article history:
Received 2 February 2013
Received in revised form
13 June 2013
Accepted 19 June 2013
Available online 28 June 2013

Keywords:
Mars
Airglow
Seasonal and latitudinal variations

ABSTRACT

An attempt has been made to detect the O_2 nightglow at 1.27 μm at low latitudes on Mars using ground-based high-resolution spectroscopy. The observed intensity is 10 ± 32 kR, that is, less than 40 kR with a probability of 83%. The current models give the O_2 nightglow intensity from 13 to 100 kR. Continuation of the ground-based observations of the O_2 dayglow at 1.27 μm in the last 3 martian years results in interannual variations of the dayglow at $L_S \approx 15^\circ$, 65°, and 110°. According to the observations, these variations are typically ~20% in northern spring and summer. Our long-term observations of the O_2 dayglow are presented as a seasonal-latitudinal map that is compared with models by Krasnopolsky (2009) and Gagne et al. (2012). While the models correctly reproduce the general behavior of the dayglow, there are some differences that are briefly discussed.

© 2013 Elsevier Ltd. All rights reserved.

1. Introduction

Nightglow is a fascinating phenomenon that reflects atmospheric chemistry and dynamics. The first attempt to detect nightglow on Mars was made in the visible range from the Mars 5 orbiter (Krasnopolsky and Krysko, 1976) and resulted in upper limits of 50 R for individual emission lines in the nadir and limb observations. (One Rayleigh is an emission of 10^6 photons per (cm^2 s 4π sr).) After the discovery of the Venus nightglow in the visible range (Krasnopolsky et al., 1976; Krasnopolsky, 1983) and in the $O_2(a^1\Delta_g \rightarrow X^3\Sigma_g^-)$ band at 1.27 μm (Connes et al., 1979), it became clear that the O_2 band at 1.27 μm is the strongest nightglow feature on the terrestrial planets. This nightglow is excited by the termolecular association of O_2 with a high yield of ~0.7 (Krasnopolsky, 2011).

The O_2 band at 1.27 μm was detected in the martian dayglow by Noxon et al. (1976) and then observed by Traub et al. (1979). This band is excited by photolysis of ozone with a yield close to one and then either emitted or quenched by CO_2 below ~20 km. Clancy and Nair (1996) argued that ozone at and above ~20 km is even more sensitive to variations of the martian photochemistry at low and middle latitudes than the column ozone. Therefore Krasnopolsky (1997) proposed ground-based observations of the O_2 dayglow at 1.27 μm as a substitute for the high-altitude ozone to monitor variations of Mars photochemistry and dynamics. The observations were made by Krasnopolsky and Bjoraker (2000), Novak et al. (2002), and Krasnopolsky (2003, 2007).

A bright O_2 1.27 μm airglow of 2.2 MR was observed 0.6 arcs off the martian nightside limb at 70°S and $L_S = 173^\circ$ (Krasnopolsky, 2003). That was probably a detection of the polar nightglow on Mars. However, Krasnopolsky (2003) pointed out contributions from three possible sources: a true nightglow, a nightside tail of the dayglow with the lifetime of 1.2 h, and a tail of the instrument response function.

The Mars Express orbiter started science observations in 2004, and two instruments, SPICAM-IR and OMEGA, have capabilities to observe the O_2 airglow at 1.27 μm. The SPICAM-IR observations for a full martian year are discussed by Fedorova et al. (2006). The results are in excellent agreement with those from the ground-based observations by Krasnopolsky (2003, 2007), especially after correction for variations with local time. Some detailed maps of the dayglow were observed by OMEGA (Altieri et al., 2009) in the subpolar regions in seasons, when the dayglow was very bright.

SPICAM-UV observations discovered an aurora (Bertaux et al., 2005a) and the NO UV nightglow (Bertaux et al., 2005b; Cox et al., 2008) that is similar to those observed on the Earth and Venus and excited by the radiative association of the NO molecule.

Recently three independent teams (Bertaux et al., 2012; Fedorova et al., 2012; Clancy et al., 2012a, 2012b) revealed a very bright emission of O_2 at 1.27 μm from winter polar night regions. The observations were made using OMEGA and SPICAM-IR at Mars Express and CRISM at the Mars Reconnaissance Orbiter (MRO), respectively. The polar nightglow intensity has a peak of ~10 MR at ~55 km on the limb with a mean vertical intensity of ~250 kR.

* Correspondence address: 6100 Westchester Park Drive #911, College Park, MD 20740, USA. Tel.: +1 240 473 6831; fax: +1 202 319 4448.
E-mail address: vlad.krasn@verizon.net

[1] Visiting Astronomer at the Infrared Telescope Facility, which is operated by the University of Hawaii under Cooperative Agreement no. NCC 5-538 with the National Aeronautic and Space Administration, Science Mission Directorate, Planetary Astronomy Program.

0032-0633/$ - see front matter © 2013 Elsevier Ltd. All rights reserved.
http://dx.doi.org/10.1016/j.pss.2013.06.018

The polar night conditions appear at latitudes exceeding 70° during winter. The observed polar nightglow agrees with simulations by the LMD general circulation model that are reproduced in the cited publications. The bright polar nightglow is excited by the termolecular association of O_2 in a descending flow of air in the Hadley circulation. This air is transported from the low and middle latitudes and enriched with atomic oxygen.

However, the polar night conditions are extreme and very different from the mean nighttime conditions on Mars. Here we will describe our attempt to detect the O_2 nightglow at 1.27 μm at low latitudes and then discuss a continuation of our observations of the O_2 dayglow for the last 3 martian years.

2. Search for O_2 nightglow at low latitudes on Mars

Our observations were conducted at the NASA Infrared Telescope Facility (IRTF) on Mauna Kea (Hawaii). The telescope diameter is 3 m, and its elevation is 4.2 km with atmospheric pressure of 0.6 bar. We applied the CSHELL spectrograph (Greene et al., 1993) that covers an interval of $0.0023\nu_0$ with resolving power $\nu/\delta\nu = 4\times10^4$. Here ν_0 is the central wavenumber that may be chosen in a range of 1800–9000 cm^{-1} (5.5–1.1 μm). The instrument detector is an InSb array of 256 × 150 pixels cooled to 30 K. The pixel size is $9\times10^{-6}\,\nu_0$ in the dispersion and 0.2 arcs in the aspect direction. Each exposure gives a frame of 150 spectra along the slit of 30 arcs with 256 pixels in each spectrum.

The observations were made on May 10, 2012, when Mars was at 1.631 AU from the Sun and 1.016 AU from the Earth. Its angular diameter was 9.2 arcs (46 pixels) and geocentric velocity was 14.0 km s^{-1}. This velocity results in a Doppler shift of −0.37 cm^{-1} at 7900 cm^{-1}. Position of Mars in the celestial coordinates is shown in Fig. 1. Mars was near the peak of northern summer with $L_S = 110°$ that corresponds to July 11 in the terrestrial calendar.

The night crescent of Mars is always small and poorly seen from the Earth. Its width was 0.9 arcs in our observations. The night crescent was morningside, and this rules out the O_2 dayglow tail caused by the long dayglow radiative time. We acquired two 8 min and one 20 min exposures to observe the nightglow at the nightside limb and ~0.5 arcs below and above the limb (Fig. 1). Spectra of dark current and flat field using a continuum source were observed as well, and the dark current was subtracted from the martian and flat field spectra. Then bad pixels in their ratio were replaced by mean values from their neighbors, and 21 spectra in each of three observing frames were summed up to improve signal-to-noise ratio. These 21 spectra are closest to the terminator and therefore brightest. Signals at the edges of these intervals of 21 aspect pixels are smaller than those in the centers typically by a factor of 2.

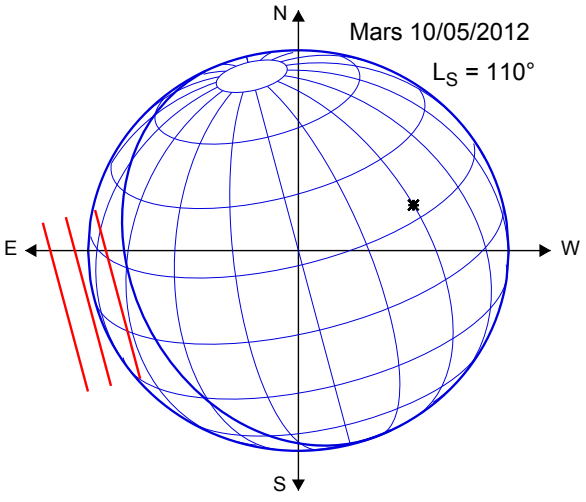

Fig. 1. Mars in the celestial coordinates during the O_2 nightglow observations. Its diameter is 9.2 arcs (46 pixels). Positions of the subsolar point, terminator, and three slits for the nightglow exposures are shown. 21 pixels were used for the nightglow measurements, and the slit length is 21 pixels in the figure. Local time at the nightside limb is 03:20.

The observed spectra at three slit positions are shown in Fig. 2. Bright continuous radiation from the dayside disk of Mars dominates in all spectra, because the dayside disk is off the instrument field of view by just a few arc seconds. Each spectrum includes eight telluric O_2 absorption lines that are identified in the lower panel. One strong line is solar, and there are some weak solar lines and lines of the martian CO_2 in the spectra. The spectra look rather similar, though that in the lower panel is weaker than that in the upper panel by a factor of 6.5.

Absolute calibration of the spectra was made observing a standard infrared star. The spectral frame for the star was also used to derive the instrument line spread function (LSF). The star continuum spectrum would be just a thin line in the spectral frame for an ideal instrument. The observed spectrum has a finite width, and its distribution in the aspect direction is the instrument LSF (Fig. 3). Generally, a point spread function may be obtained from the observed LSF, but we do not need it.

Our observations of the O_2 dayglow along the central meridian on the same date will be discussed in the next section. Using the measured continuum brightness and assuming the Lambert reflection of the solar light from the surface and lower atmosphere, we calculated brightness distribution along the martian disk. We convolved this distribution using the observed LSF and obtained a brightness distribution seen by our instrument off the terminator. Comparing the calculated distribution with the observed spectra in Fig. 2, we got more accurate positions of the slits during the observations than those extracted from the telescope data. They are shown in Fig. 1. The O_2 nightglow is expected at 50–65 km at low latitudes on Mars. Absorption by dust and haze is weak at these altitudes and may be safely neglected.

All telluric O_2 lines show some asymmetry and excess on the left shoulder that is due to the Doppler shifted martian emission. We choose four lines to extract the martian airglow. They are marked red in Fig. 2. The other four lines are either contaminated or weak. Our technique of the martian O_2 airglow extraction is similar to that used in our previous observations (Krasnopolsky, 2003). The observed line shape is fitted by a sum of Gaussian and parabola (Fig. 4). Five pixels that are centered at the expected Doppler-shifted position of the martian airglow line are not involved in the fitting, and a difference between these pixels and the calculated fit gives the airglow line intensity.

The radiative lifetime of $O_2(a^1\Delta_g)$ is long, and rotational temperature of the O_2 nightglow at 1.27 μm should be similar to the ambient temperature of the atmosphere. We will see below that the O_2 dayglow from the dayside disk of Mars at tail of LSF dominates in the extracted O_2 emission lines. Its mean temperature is

$$T = \frac{\int_0^\infty T(h)i(h)dh}{\int_0^\infty i(h)dh}$$

where $i(h)$ is the O_2 dayglow volume emission rate, and the data from our model at $L_S = 112°$ and 20°N (Krasnopolsky, 2006, figure 10) result in $T = 172$ K.

Line intensity is proportional to $Ag_u e^{-\alpha(E_0+\upsilon)/T}$, where A is the line transition probability, g_u is the statistical weight of the upper state, $\alpha = 1.4388$ cm K, E_0 is the lower state energy in cm^{-1}, and ν is the line wavenumber. All these values may be found in HITRAN 2008 (Rothman et al., 2009). According to this relationship, the chosen O_2 lines at 7888.06, 7893.53, 7895.48, and 7900.83 cm^{-1}

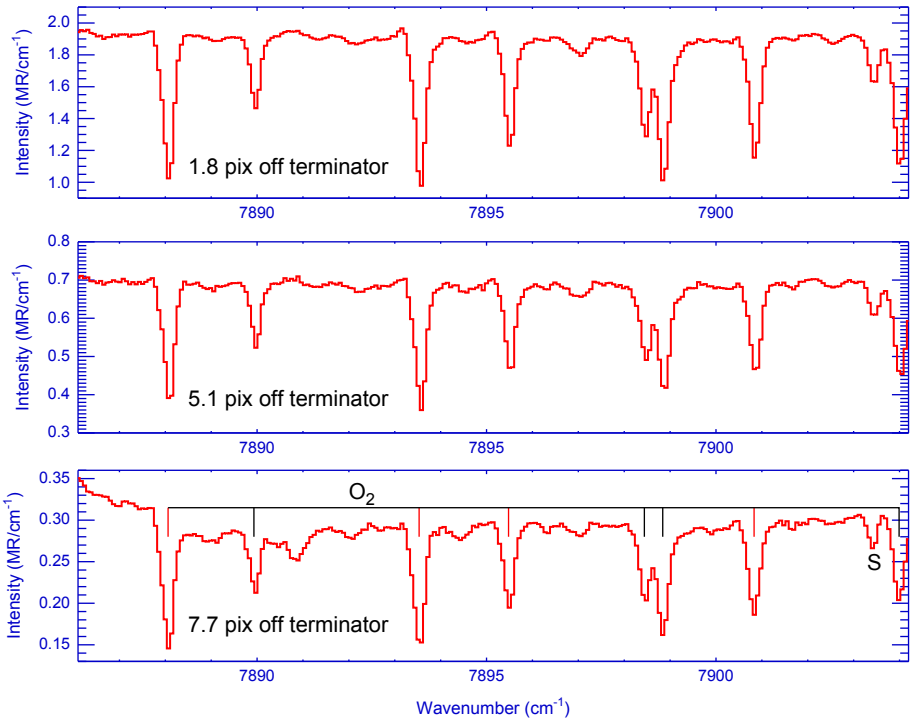

Fig. 2. Averaged spectra observed near the martian nightside limb. Positions of eight telluric O_2 lines and a solar line S are shown. Other features are weak solar lines and martian CO_2 lines. Four O_2 lines that are used for extraction of the martian O_2 airglow are marked red in the lower panel. (For interpretation of the references to color in this figure legend, the reader is referred to the web version of this article.)

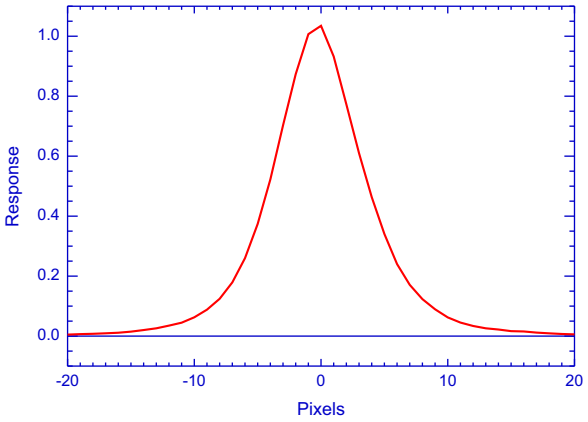

Fig. 3. The instrument line spread function extracted from the star spectra.

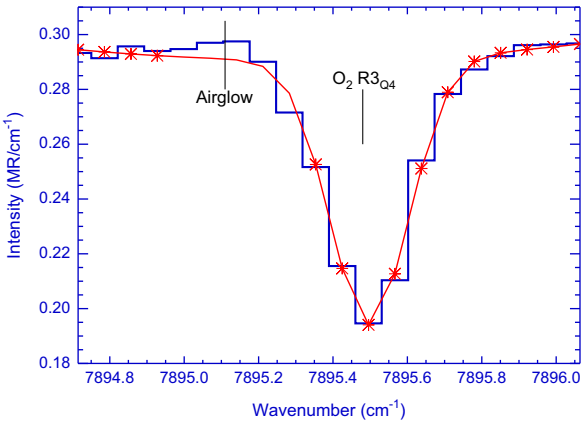

Fig. 4. Fitting of the O_2 line at 7895.48 cm^{-1} from the spectrum in the lower panel of Fig. 2 by a sum of Gaussian and parabola. Five pixels centered at the expected Doppler-shifted position of the martian airglow line are not involved in the fitting. Difference between these five observed pixels and their fitting values is equal to the airglow line intensity. Pixels involved in the fitting are marked by asterisks.

constitute 3.48%, 3.66%, 2.21%, and 2.31% of the total O_2 dayglow at 172 K respectively. Using these values, the extracted line intensities are converted into the total airglow intensities. We obtain four total airglow intensities for each slit position, and their mean values are shown in Fig. 5. Their uncertainties are equal to standard deviations of the four values divided by $(4-1)^{1/2}$ and shown in Fig. 5 as well. Uncertainties associated with the dayglow temperature of 172 K are much smaller than those shown in Fig. 5.

The retrieved O_2 airglow intensities are compared in Fig. 5 with brightness factors $\pi I/I_0$ in the spectra, where I is the continuum radiation in the spectra and I_0 is the solar radiation at 1.27 μm at Mars' orbit; $I_0=436$ erg cm^{-2} s^{-1} nm^{-1} at 1 AU (Pierce and Allen, 1977). Brightness factor is a ratio of the observed brightness to that of a normally illuminated perfect Lambert surface. Ratios of the O_2 airglow intensities and the brightness factors are constant within the uncertainties for all slit positions; therefore the nightglow contribution is within the observational uncertainties.

To evaluate the effect of the O_2 nightglow, we assumed a uniform nightglow layer of 100 kR between 50 and 65 km. Models (see Section 4.1) predict the O_2 nightglow excited by the termolecular association of oxygen at these altitudes. Then the airglow intensity distribution was calculated along the disk and on the limb with reflection from the martian surface and lower atmosphere taken into account. This distribution was convolved by LSF to give expected intensities at the positions of the instrument slit during the observations (Fig. 5). Each pixel is 0.2 arcs or 148 km, LSF is even wider, and the calculated curve is insensitive to the adopted shape of the nightglow layer.

The observed airglow intensity is a sum of the brightness factor and the convolved nightglow, both scaled by some factors. We have three simple equations with two unknown factors. The data for the first and second slits result in a nightglow vertical intensity

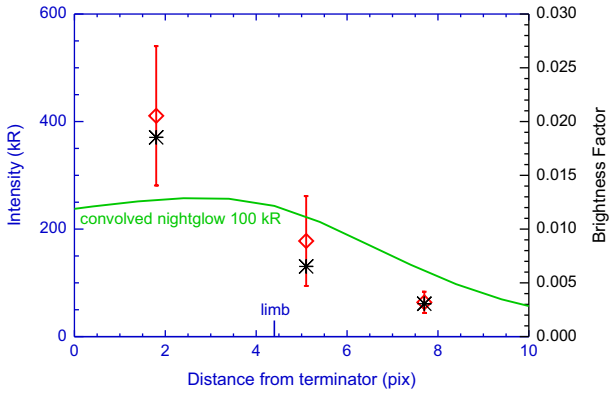

Fig. 5. O_2 airglow intensities (red diamonds) and brightness factors (black asterisks) extracted from the observed spectra in Fig. 2. Convolution of the calculated O_2 nightglow with vertical intensity of 100 kR is also shown. (For interpretation of the references to color in this figure legend, the reader is referred to the web version of this article.)

of 25 ± 72 kR; the data for the first and third slits give -5 ± 36 kR. The weighted mean of these values is the vertical intensity of the O_2 nightglow at 1.27 μm equal to 10 ± 32 kR. Therefore, the O_2 nightglow has not been detected in our observation. The observation was made at $L_S = 110°$, covered latitudes of $\pm 20°$, and local time was 03:20 at the nightside limb.

3. Observations of the O_2 dayglow at 1.27 μm

The O_2 dayglow is excited by photolysis of ozone with a rate coefficient $J = 0.0082\ s^{-1}$ at 1 AU and then either emitted with radiative lifetime $\tau = 4460$ s (Lafferty et al., 1998) or quenched by CO_2. An upper limit of $2 \times 10^{-20}\ cm^3\ s^{-1}$ is given to the quenching coefficient by Sander et al. (2011). Two versions of our model (Krasnopolsky, 2006, 2009) applied either $k = 2 \times 10^{-20}\ cm^3\ s^{-1}$ to agree the O_2 dayglow with ground-based (Fast et al., 2006) and HST (Clancy et al., 1999) observations of ozone or $k = 5 \times 10^{-21}\ cm^3\ s^{-1}$ to fit the SPICAM/MEX observations of ozone (Perrier et al., 2006). The dayglow vertical intensity is

$$4\pi I(MR) = \frac{10^{-12} J}{r_h^2} \int_0^\infty \frac{[O_3]dh}{1 + \tau k[CO_2]}$$

where r_h is Mars heliocentric distance in AU. The quenching becomes weak above ~20 km, and the O_2 dayglow is sometimes considered as an equivalent of column ozone above 15–20 km. However, ozone densities may significantly grow down to the surface and compensate for the increasing quenching. Therefore the conversion of the O_2 dayglow intensity to high-altitude ozone is typically very uncertain, and the O_2 dayglow should be treated as an independent tracer of Mars photochemistry, along with column O_3 and H_2O_2.

Our ground-based high-resolution observations of the O_2 dayglow before 2007 are discussed in Krasnopolsky (2007). The observed emissions are measurable against the O_2 telluric absorption lines if Mars geocentric velocity exceeds ~10 km s^{-1}. The observations are preferable when Mars diameter is greater than ~8 arcs. These requirements restrict favorable observing periods to a month 2 months before and after the opposition. The oppositions occur with a period of ~2.15 years, and this results in the observing rate of ~1 session per year. Dates and conditions of our observations are given in Table 1.

Some observing sessions were made at similar martian seasons, and this makes it possible to compare the data and evaluate interannual variations of the O_2 dayglow (Fig. 6). The dayglow in early spring ($L_S \approx 15°$, the upper panel) is constant at ~2 MR at the low latitudes and increases to ~10 MR at and above 50–60°. The observations near aphelion ($L_S = 60$–$70°$, the middle panel) are rather similar in March 2010 and January 2012 and smaller than those in January 1997 by a factor of ~1.5. The dayglow is almost constant at ~5.5 MR from 60°S to the North Pole. The mean dayglow is constant at ~3 MR from 60°S to 30°N and gradually decreases to 2 MR at the North Pole in summer at $L_S = 111°$ (the lower panel).

Table 1
Observations of the O_2 dayglow at 1.27 μm.

L_S	Date	Diameter[a]	Velocity[b]	Central latitude	LT[c]
10	10/02/2006	8.1	17.3	13°S	9:42
20	07/12/2009	10.4	−13.0	19°N	14:12
42	09/03/2008	8.4	17.1	2°N	9:48
60	22/01/2012	10.9	−13.2	23°N	14:00
68	21/01/1997	9.7	−15.1	23°N	14:18
70	31/03/2010	9.3	15.4	14°N	9:44
110	10/05/2012	9.2	14.0	24°N	9:20
112	20/03/1999	12.6	−12.9	15°N	13:38
148	20/04/2001	12.8	−13.8	1°S	14:00
173	23/04/2003	8.9	−14.4	15°S	14:36
247	10/07/2005	9.9	−10.1	22°S	15:25
312	08/12/2003	10.3	14.5	26°S	9:00
331	18/10/2007	11.0	-11.3	6°N	14:24

[a] Mars diameter in arcs.
[b] Mars geocentric velocity that determines the Doppler shift (km s^{-1}).
[c] Local time at the central meridian.

Our observations of the O_2 dayglow on Mars are typically made at the central meridian that is usually near LT 14:00 and 10:00 before and after the opposition, respectively (Table 1). The O_2 dayglow at low latitudes is maximal near noon and weaker by a factor of ~3 at 8:00 and 18:00 (Krasnopolsky, 2003). However, according to our observations, the O_2 dayglow variations with local time are different at various latitudes and seasons. Corrections for local time to the data in Fig. 6 are therefore uncertain, do not reduce the scatter of the data, and are not shown.

Standard deviation for the data of the curves in Fig. 6 at the same latitude may serve as an assessment of interannual variability of the O_2 dayglow. Its mean value is 22%.

A map of the seasonal and latitudinal variations of the O_2 dayglow is shown in Fig. 7. This map is based on all our observations. The map reflects the dayglow behavior discussed above for $L_S \leq 110°$. The dayglow intensity decreases from ~3 MR at $L_S = 110°$ to ~1 MR at $L_S = 200$–$320°$. Significant intensities ~10 MR and higher may be observed at the south subpolar latitudes near the fall equinox. Overall, the dayglow varies at the low and middle latitudes from ~6 MR near aphelion ($L_S = 71°$) to ~1 MR near perihelion ($L_S = 251°$), and the bright dayglow ~10 MR is typical of latitudes exceeding 40°S and N near the spring equinox.

4. Discussion

4.1. O_2 nightglow

The O_2 nightglow at 1.27 μm is excited by the termolecular association of O_2. The extracted O_2 nightglow of 10 ± 32 kR means, for example, that the nightglow vertical intensity does not exceed 40 kR with probability of 83%. The published OMEGA and SPICAM-IR observations from Mars Express (Bertaux et al., 2012; Fedorova et al., 2012) and CRISM/MRO observations (Clancy et al., 2012a) refer to the polar nightglow, that is, to the nightglow from regions of the winter polar night. The mean O_2 vertical nightglow intensity is 250 kR in all three publications. Recently the OH polar nightglow was detected by CRISM/MRO as well (Clancy et al., 2012b).

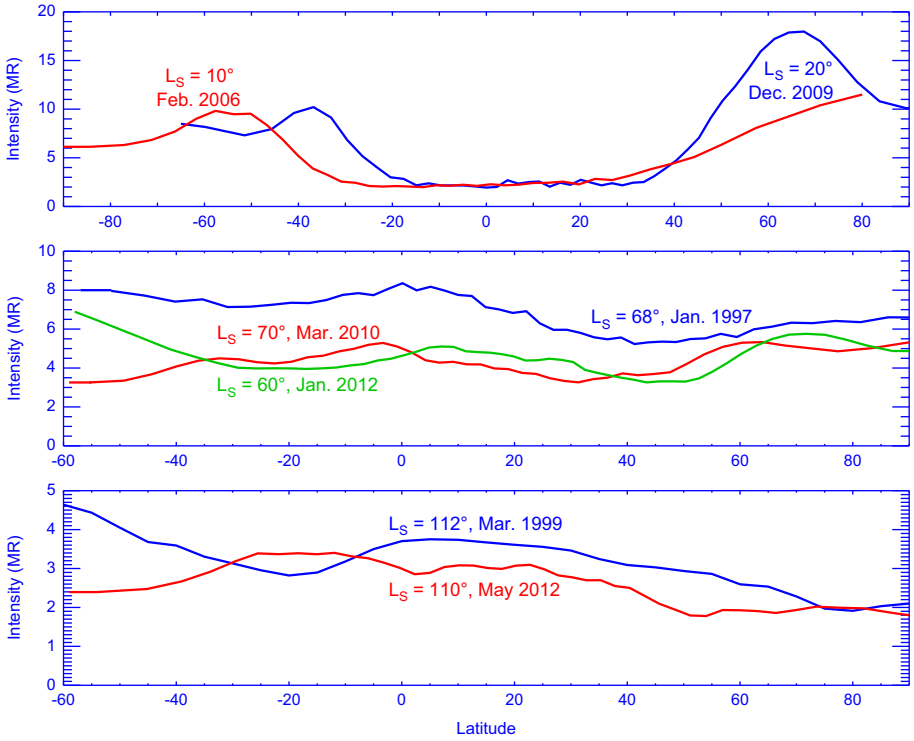

Fig. 6. Observed interannual variations of the O_2 dayglow at 1.27 μm on Mars.

However, there are no published observations of the O_2 nightglow at 1.27 μm at the low and middle latitudes.

Modeling of the O_2 nightglow at the low latitudes was made by Garcia Munoz et al. (2005), Krasnopolsky (2006, 2011), Zhu and Yee (2007), and Gagne et al. (2012). The nightglow intensity is constant during the night and equal to 27 kR in Garcia Munoz et al. (2005) with a peak altitude of 62 km. Their model was calculated for the Mars mean heliocentric distance of 1.52 AU and latitude of 20°.

The O_2 nightglow was calculated by Krasnopolsky (2006) for the equator near the fall equinox and 20°N (subsolar latitude) at L_S=112°. The calculated intensities are scaled in Krasnopolsky (2011) by a factor of 1.5 to account for a recently measured rate coefficient of the termolecular association of O_2 (Smith and Robertson, 2008) that excited the O_2 nightglow. The calculated O_2 nightglow varies during the night by a factor of ~3 with mean corrected intensities of 13 and 30 kR. The nightglow peak is near 58 km. Our evaluation of the nightglow intensity at midnight in a figure from Zhu and Yee (2007) is ~15 kR with a peak at 57 km.

The models by Garcia Munoz et al. (2005), Krasnopolsky (2006), and Zhu and Yee (2007) are time-dependent and one-dimensional. Zhu and Yee (2007) adopted photochemical equilibrium $n_i = P_i/L_i$ as boundary conditions for all species except CO_2, H_2O, CO, O_2, and H_2. Closed boundaries with zero fluxes are used for these species in the other models, that is, the species do not react with the surface rocks. The conditions of photochemical equilibrium at the surface actually mean unspecified sources or sinks of the species on the surface. Maybe, that is why the ozone profile in Zhu and Yee (2007) is very different from those in the other models.

The results of Gagne et al. (2012) are based on the LMD GCM (Lefèvre et al., 2008; González-Galindo et al., 2009). The calculated nightglow at midnight and at the low and middle latitudes is at the lowest color grade of less than 100 kR in all seasons. Detailed data are given for the equator at midnight at L_S=0° and 180°. Temperature profiles for both seasons are similar with a minimum

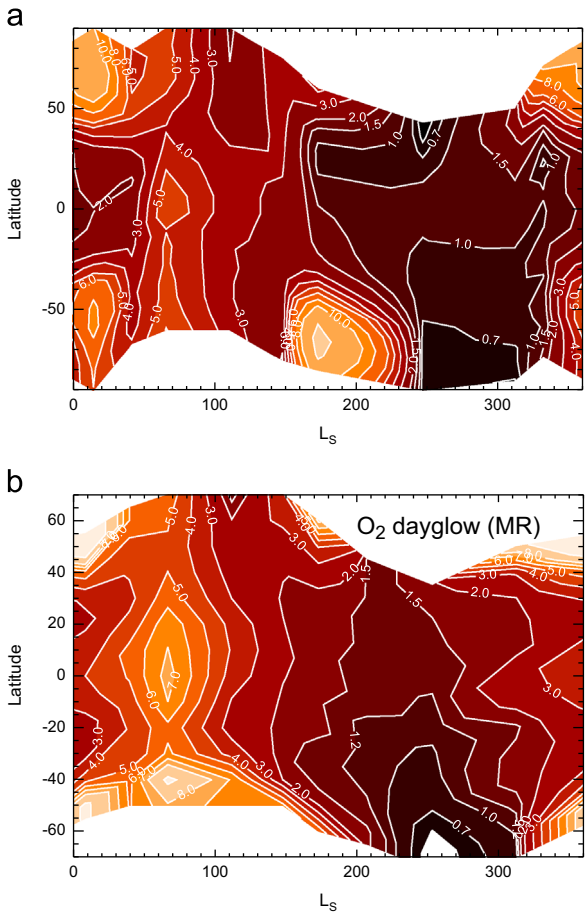

Fig. 7. Maps of seasonal and latitudinal variations of the O_2 dayglow at 1.27 μm (intensities in MR): our observations (upper panel) and model (lower panel, (Krasnopolsky, 2009)).

of 140 K at 55 km and a maximum of 170 K at 75 km. However, this warm nightside layer is not seen in the SPICAM/MEX stellar occultations (Forget et al., 2009) and in the MCS/MRO observations (McCleese et al., 2010). Atomic oxygen peaks at 75 km with significant densities down to ~50 km in the model, and this results in a two-layer structure of the nightglow, because CO_2 is much more abundant at 50 km than at 75 km. The layer peaks are at 55 and 79 km. The nightglow vertical intensities are not given in the paper; our evaluations of data in their figure are 20 kR at $L_S=0^\circ$ and 38 kR at $L_S=180^\circ$. Therefore, the model nightglow intensities are within the large uncertainty of our observation.

4.2. O_2 dayglow

The seasonal-latitudinal map of the observed O_2 dayglow is compared in Fig. 7 with that from our model (Krasnopolsky, 2009). The model is one-dimensional but based on 3D data of TES/MGS on temperature profiles and H_2O, dust, and ice columns (Smith, 2004). The model is zonal-mean and accounts for variations of the solar flux with solar zenith angle, duration of day, and heliocentric distance. The 1D model results are applicable if local productions and losses of species exceed their net deliveries by horizontal winds. The TES H_2O data are lacking at high latitudes, and this restricts the model as well. We expect that both restrictions are rather similar, and the data shown may be considered with some confidence.

There are some differences between the model and the observations. The model does not reproduce a peak at ~60°S near the fall equinox. However, this point is near the south boundary of the model. On the other hand, this strong emission agrees with the OMEGA/MEX observations at the subpolar latitudes near equinoxes (Altieri et al., 2009). The dayglow increase at ~40°S near aphelion is steeper in the model than that observed. Overall, the agreement between the observations and the model may be considered as very good.

Gagne et al. (2012) computed a map of seasonal-latitudinal variations of the O_2 dayglow based on the LMD GCM. The map reproduces main features of the dayglow variations shown in Fig. 7 and discussed above. Furthermore, the map covers the polar regions that are beyond our observations and model for some seasons. There are some differences between the map in Gagne et al. (2012) and our observations. The dayglow near aphelion is ~30 MR at 40–45°S and decreases to ~2 MR at the North Pole in Gagne et al. (2012), while it is rather stable at ~6 MR from 60°S to the North Pole in our observations (Fig. 6). The dayglow is ~2 MR during fall and winter from ~60°S to ~35°N in Gagne et al. (2012) and ~1 MR in our observations and model (Fig. 7).

5. Conclusions

Our attempt to detect the O_2 nightglow at 1.27 μm at low latitudes results in its intensity of 10 ± 32 kR, that is, less than 40 kR with probability of 83%. The uncertainty covers the current models that give the O_2 nightglow intensity from 13 to 100 kR at low latitudes.

We continued our ground-based observations of the O_2 dayglow at 1.27 μm in the last 3 martian years. Interannual variations of the dayglow were observed at $L_S \approx 15^\circ$, 65°, and 110°. We conclude that these variations are typically ~20% in northern spring and summer.

The results of the long-term observations of the O_2 dayglow are presented as a seasonal-latitudinal map that is compared with similar maps calculated by Krasnopolsky (2009) and Gagne et al. (2012). While the models correctly reproduce the general behavior of the dayglow, there are some differences that are briefly discussed.

Acknowledgment

This work is supported by a grant of the NASA Planetary Astronomy Program to V.A. Krasnopolsky and a grant of the Russian Government to MIPT and V.A. Krasnopolsky.

References

Altieri, F., Zasova, L., d'Aversa, E., Bellucci, G., Carrozzo, F.G., Gondet, B., Bibring, J.P., 2009. O_2 1.27 μm emission maps as derived from OMEGA/MEX data. Icarus 204, 499–511.

Bertaux, J.L., Leblanc, F., Witasse, O., Quemerais, E., Lilensten, J., Stern, A., Sandel, B., Korablev, O., 2005a. Discovery of an aurora on Mars. Nature 435, 790–794.

Bertaux, J.L., et al., 2005b. Nightglow in the upper atmosphere of Mars and implications for atmospheric transport. Science 307, 566–569.

Bertaux, J.-L., Gondet, B., Bibring, J., Montmessin, F., Lefèvre, F., 2012. First detection of O2 1.27-mm nightglow emission at Mars with OMEGA/MEX and comparison with general circulation model predictions. Journal of Geophysical Research 117, E00J04, http://dx.doi.org/10.1029/2011JE003890.

Clancy, R.T., Nair, H., 1996. Annual (perihelion–aphelion) cycles in the photochemical behavior of the global Mars atmosphere. Journal of Geophysical Research 101, 12785–12790.

Clancy, R.T., Wolff, M.J., James, P.B., 1999. Minimal aerosol loading and global increase in atmospheric ozone during the 1996–1997 martian northern spring season. Icarus 138, 49–63.

Clancy, R.T., et al., 2012a. Extensive MRO CRISM observations of 1.27 μm O_2 airglow in Mars polar night and their comparison to MRO MCS temperature profiles and LMD GCM simulations. Journal of Geophysical Research 117, E00J10, http://dx.doi.org/10.1029/2011JE004018.

Clancy, R.T., Sandor, B.J., Garcia Munoz, A., Lefevre, F., Smith, M.D., Wolff, M.J., Murchie, S.L., 2012b. OH Meinel Band Polar Nightglow in the Mars Atmosphere from MRO CRISM Limb Observations. AGU Fall Meeting, Abstract 1464823.

Connes, P., Noxon, J.F., Traub, W.A., Carleton, N.P., 1979. O2($^1\Delta_g$) emission in the day and night airglow of Venus. Astrophysical Journal 233, L29–L32.

Cox, C., Saglam, A., Gérard, J.C., Bertaux, J.L., González-Galindo, F., Leblanc, F., Reberac, A., 2008. Distribution of the ultraviolet nitric oxide Martian night airglow: observations from Mars Express and comparisons with a one-dimensional model. Journal of Geophysical Research 113, E08012.

Fast, K.E., Kostiuk, T., Espenak, F., Annen, J., Buhl, D., Hewagama, T., et al., 2006. Ozone abundance on Mars from infrared heterodyne spectra. I. Acquisition, retrieval, and anticorrelation with water vapor. Icarus 181, 419–431.

Fedorova, A., Korablev, O., Perrier, S., Bertaux, J.L., Lefevre, F., Rodin, A., 2006. Observations of O_2 1.27 μm dayglow by SPICAM IR: seasonal distribution for the first Martian year of Mars Express. Journal of Geophysical Research 111, E09S07.

Fedorova, A.A., Guslyakova, S., Lefèvre, F., Bertaux, J.L., Korablev, O., Montmessin, F., Reberac, A., Gondet, B., 2012. The O_2 nightglow in the Martian atmosphere by SPICAM onboard of Mars-Express. Icarus 219, 596–608.

Forget, F., Montmessin, F., Bertaux, J.L., González-Galindo, F., Lebonnois, B., Quémerais, E., Reberac, A., Dimarellis, E., López-Valverde, M.A., 2009. Density and temperatures of the upper Martian atmosphere measured by stellar occultations with Mars Express SPICAM. Journal of Geophysical Research 114, E01004, http://dx.doi.org/10.1029/2008JE003086.

Gagne, M.E., Melo, S.M.L., Lefevre, F., Gonzalez-Galindo, F., Strong, K., 2012. Modeled O_2 airglow distributions in the Martian atmosphere. Journal of Geophysical Research 117, E06005, http://dx.doi.org/10.1029/2011JE003901.

Garcia Munoz, A., McConnell, J.C., McDade, I.C., Melo, S.M.L., 2005. Airglow on Mars: some model expectations for the OH Meinel bands and the O_2 IR atmospheric band. Icarus 176, 75–95.

González-Galindo, F., Forget, F., López-Valverde, M.A., Angelats i Coll, M., Millour, E., 2009. A ground-to-exosphere Martian general circulation model: 1. Seasonal, diurnal, and solar cycle variation of thermospheric temperatures. Journal of Geophysical Research 114, E04001, http://dx.doi.org/10.1029/2008JE003246.

Greene, T.P., Tokunaga, A.T., Toomey, D.W., Carr, J.S., 1993. CSHELL: A high spectral resolution echelle spectrograph for the IRTF. Proceedings of SPIE 1946, 313–323.

Krasnopolsky, V.A., 1983. Venus Spectroscopy in the 3000–8000 Å Region by Veneras 9 and 10. In: Hunten, D.M., Colin, L., Donahue, T.M., Moroz, V.I. (Eds.), Venus. University Arizona Press, Tucson, AZ, pp. 459–483.

Krasnopolsky, V.A., 1997. Photochemical mapping of Mars. Journal of Geophysical Research 102, 13113–13320.

Krasnopolsky, V.A., 2003. Mapping of Mars O_2 1.27 μm dayglow at four seasonal points. Icarus 165, 315–325.

Krasnopolsky, V.A., 2006. Photochemistry of the martian atmosphere: seasonal, latitudinal, and diurnal variations. Icarus 185, 153–170.

Krasnopolsky, V.A., 2007. Long-term spectroscopic observations of Mars using IRTF/CSHELL: mapping of O_2 dayglow, CO, and search for CH_4. Icarus 190, 93–102.

Krasnopolsky, V.A., 2009. Seasonal variations of photochemical tracers at low and middle latitudes on Mars: observations and models. Icarus 201, 564–569.
Krasnopolsky, V.A., 2011. Excitation of the oxygen nightglow on the terrestrial planets. Planetary and Space Science 59, 754–766, http://dx.doi.org/10.1016/j.pss.2011.02.015.
Krasnopolsky, V.A., Bjoraker, G.L., 2000. Mapping of Mars $O_2(^1\Delta)$ dayglow. Journal of Geophysical Research 105, 20179–20188.
Krasnopolsky, V.A., Krysko, A.A., 1976. On the night airglow of the martian atmosphere. Space Research 16, 1005–1008.
Krasnopolsky, V.A., Krysko, A.A., Rogachev, V.N., Parshev, V.A., 1976. Spectroscopy of the Venus night airglow from the Venera 9 and 10 orbiters. Cosmic Research 14, 789–795.
Lafferty, W.J., Solodov, A.M., Lugez, C.L., Fraser, G.T., 1998. Rotational line strengths and self-pressure broadening coefficients for the 1.27-μm, $a^1\Delta_g$–$X^3\Sigma_g$, v=0–0 band of O_2. Applied Optics 37, 2264–2270.
Lefèvre, F., Bertaux, J.L., Clancy, R.T., Encrenaz, T., Fast, K., Forget, F., Lebonnois, S., Montmessin, F., Perrier, S., 2008. Heterogeneous chemistry in the atmosphere of Mars. Nature 454 (7207), 971–975.
McCleese, D.J., et al., 2010. Structure and dynamics of the Martian lower and middle atmosphere as observed by the Mars Climate Sounder: seasonal variations in zonal mean temperature, dust, and water ice aerosols. Journal of Geophysical Research 115, E12016, http://dx.doi.org/10.1029/2010JE003677.
Novak, R.E., Mumma, M.J., DiSanti, M.A., Dello Russo, N., Magee-Sauer, K., 2002. Mapping of ozone and water in the atmosphere of Mars near the 1997 aphelion. Icarus 158, 14–23.
Noxon, J.F., Traub, W.A., Carleton, N.P., Connes, P., 1976. Detection of O_2 dayglow emission from Mars and the Mars ozone abundance. Astrophysical Journal 207, 1025–1031.
Perrier, S., Bertaux, J.L., Lebonnois, S., Korablev, O., Fedorova, A., 2006. Global distribution of total ozone on Mars from SPICAM/MEX UV measurements. Journal of Geophysical Research 111, E09S06, http://dx.doi.org/10.1029/2006JE002681.
Pierce, A.K., Allen, R.G., 1977. The solar spectrum between 0.3 and 10 μm. In: White, O.R. (Ed.), The Solar Output and its Variations. Colo. Assoc. Univ. Press, Boulder, pp. 169–192.
Rothman, L.S., Gordon, I.E., Barbe, A., Benner, D.C., Bernath, P.F., Birk, M., et al., 2009. The HITRAN 2008 molecular spectroscopic database. Journal of Quantitative Spectroscopy and Radiative Transfer 110, 533–572.
Sander, S.P. et al., 2011. Chemical Kinetics and Photochemical Data for Use in Atmospheric Studies. Evaluation Number 17. JPL Publication 10-6.
Smith, G.P., Robertson, R., 2008. Temperature dependence of oxygen atom recombination in nitrogen after ozone photolysis. Chemical Physics Letters 458, 6–10.
Smith, M.D., 2004. Interannual variability in TES atmospheric observations of Mars during 1999–2003. Icarus 167, 148–165.
Traub, W.A., Carleton, N.P., Connes, P., Noxon, J.F., 1979. The latitude variation of O_2 dayglow and O_3 abundance on Mars. Astrophysical Journal 229, 846–854.
Zhu, X., Yee, J.H., 2007. Wave-photochemistry coupling and its effect on water vapor, ozone and airglow variations in the atmosphere of Mars. Icarus 189, 136–150.